Surv Geophys
DOI 10.1007/s10712-014-9305-z

The Effect of Shallow Quaternary Deposits on the Shape of the H/V Spectral Ratio

A. Macau · B. Benjumea · A. Gabàs · S. Figueras · M. Vilà

Received: 13 March 2014 / Accepted: 20 August 2014

Abstract In the last two decades, the horizontal-to-vertical (H/V) spectral ratio of seismic noise technique has been widely used for site-effect estimation and geophysical exploration through the soil fundamental frequency. Usually, only one peak is observed in the H/V spectral ratio, but in some cases, a second peak can also be obtained. Nevertheless, to date, the peaks at higher frequencies are rarely studied in detail. Geological and geophysical data are especially needed to better explain the presence of this second peak, which normally is neglected. An extensive survey of H/V measurements was conducted in the Llobregat river delta, located to the south of Barcelona. At most sites, two clear peaks were identified: one at low frequencies (<1 Hz) and the other at higher frequencies (>1 Hz). To understand this behaviour, a seismic noise array and active surface wave measurements have been conducted to obtain a shear-wave velocity profile (V_s) up to the bedrock. Two impedance contrasts have been detected: the first one at a shallow depth and the second one between the soft sedimentary cover and the bedrock. During the modelling process, the theoretical H/V computed from the obtained V_s models fits well with the experimental H/V peaks. The results from this study show that the structure of shallow quaternary layers can clearly change the shape of the H/V ratio, producing two clear peaks in some situations. In this case, the contact between the low-velocity clay layer and the gravels with a high seismic wave velocity produces a shallow impedance contrast related to the second peak observed in the H/V ratio. Comprehension of these secondary peaks could avoid a misreading of the soil fundamental frequency that could produce errors in a site-effect evaluation or in the calculation of the bedrock depth. Finally, we show that passive seismic techniques provide the quaternary overburden and bedrock geometry in urban areas and allow for the limitations of other geophysical techniques in these environments to be overcome.

Keywords Seismic noise · Surface waves · H/V method · H/V shape · Array measurements · Quaternary layers

A. Macau (✉) · B. Benjumea · A. Gabàs · S. Figueras · M. Vilà
Institut Cartogràfic i Geològic de Catalunya, Parc de Montjuïc, 08038 Barcelona, Spain
e-mail: albert.macau@icgc.cat

Published online: 26 September 2014

1 Introduction

Understanding the geological architecture of the Mediterranean deltas is essential, as they constitute unstable sedimentary systems usually subjected to high population stress (Stanley 2001). In this context, their characterisation is relevant to different fields, such as the exploitation and protection of groundwater resources or earthquake ground-motion amplification studies due to soft sediments.

The Llobregat delta (NE of the Iberian Peninsula) is strategically relevant to the Barcelona urban area and the surroundings, as it supports a major industrial settlement together with transportation infrastructures, such as highways, railways, the Barcelona harbour and the airport. In addition, the Llobregat delta represents one of the most important surface and groundwater resources in this area (Custodio 2012).

Most geological loggings conducted in the Llobregat delta are restricted to the Quaternary sediments due to their strategic importance in engineering constructions or water resources (Gámez et al. 2009). The meticulous reviews of the publications addressing the geology of the Llobregat delta (e.g., Lafuerza et al. 2005; ICC-IGC-CUADLL 2006; Liquete et al. 2008; Gámez et al. 2009 and references therein) note that, currently, few boreholes have reached the pre-Quaternary basement in the emerging delta. In the central part of the delta, there are kilometric areas without any borehole that has crossed the summit of the pre-Quaternary basement. From a geophysical point of view, the intensive urbanisation makes more difficult the use of electromagnetic surveys to image deep structures and faults due to the low-quality data (Jie et al. 2000). In addition, the presence of salt water intrusion masks the lithological–electrical resistivity relationship because the electrical properties heavily depend on the fluid content (Falgàs et al. 2011; Slater et al. 2000; Nguyen et al. 2009). On the other hand, P-wave seismic surveys revealed a strong signal attenuation due to the presence of organic material (Benjumea et al. 2006).

To study the structure of subsoil, passive seismic techniques are proposed as alternative techniques in a deltaic environment to characterise the sediments on top of the bedrock. One of these passive techniques is the horizontal-to-vertical (H/V) spectral ratio of seismic noise proposed by Nogoshi and Igarashi (1970, 1971). The H/V method computes the ratio between the Fourier amplitude spectra of the horizontal and vertical components of seismic noise measurements. It is generally accepted that this spectral ratio provides a good estimation of the soil fundamental frequency (f0). Revised by Nakamura (1989), this quick, reliable and low-cost technique has been applied in many regions for site-effect estimation (Lermo and Chávez-García 1993; Bard 1999; Fäh et al. 2001; Bonnefoy-Claudet et al. 2009; Castellaro and Mulargia 2009).

Recently, the H/V method has been highly recommended within the SESAME project (site-effect assessment using ambient excitations) after a detailed study of its implications (Bonnefoy-Claudet et al. 2006; Bard 2008; Chatelain et al. 2008; Haghshenas et al. 2008). The application of this method is particularly suitable for regions with low seismicity because it is difficult to record a convenient number of earthquakes at rock and sediment stations in a short period of time to obtain an empirical transfer function of the soil locations, as is the case in Barcelona (Lachet and Bard 1994; Cadet et al. 2011; Goded et al. 2012). From this methodology, fundamental frequencies can be obtained, but it is important to consider that the H/V ratio amplitudes cannot be related to actual soil amplification factors due to the effect of the local seismic noise sources on the H/V amplitude (Lermo and Chávez-García 1993; Cid et al. 2001; Le Brun et al. 2001; Bonnefoy-Claudet et al. 2006).

In addition to site-effect assessment, the H/V seismic noise technique has been tested as a fast and efficient way to obtain the bedrock geometry as a geophysical exploration method (Ibs-von Seht and Wohlenberg 1999; Delgado et al. 2000; Parolai et al. 2002). This method uses a f_0-bedrock depth empirical relationship to calculate the overburden thickness. Some studies have verified that the joint interpretation of H/V surveys and traditional geophysical methods provides more insights and reduces the uncertainties in surface models, becoming an effective tool for recognising and characterising the lithologies and structures of subsoil (Kühn et al. 2010; Benjumea et al. 2011; Gabàs et al. 2014).

The other passive method included in this work is the array technique. This technique records simultaneous seismic noises with multiple seismometers forming a geometry, such as triangles or circles. In recent years, the array technique has become a widespread tool to compute shear-wave velocity (V_s) (Asten and Henstridge 1984). This success comes from the easiness to use passive sources as well as from the possibility of investigating deep sedimentary structures at a lower cost compared with cross-hole, downhole or S-wave refraction techniques. The main assumptions behind an array analysis are that seismic noise is mostly composed of surface waves and that the ground structure is approximately horizontally stratified (Tokimatsu 1997). In a one-dimensional heterogeneous medium, surface waves are dispersive and show a variation in the apparent velocity with frequency. The data processing for obtaining a V_s profile from noise array measurements is divided into two main steps: deriving the spectral curve characteristics of the propagating waves (namely, a dispersion curve or auto-correlation curves) and inverting this curve to retrieve the soil structure.

The objective of this paper is to discuss and demonstrate the ability of combined passive seismic techniques (H/V and array) to detect the bedrock depth and to characterise the sediments structure in a deltaic environment where other geophysical techniques failed due to the specific characteristics of this sedimentary medium (organic sediments, saline intrusion, etc.). To achieve this objective, the following steps have been performed:

(a) Review the available passive seismic information
(b) Correlate and interpret the previous and new H/V data with borehole information
(c) Evaluate the shape of the H/V spectral ratio of the new data
(d) Analyse the new array data to provide the shear-wave velocity information of the quaternary and neogene layers up to the bedrock
(e) Obtain new and relevant interpretation of the sedimentary delta system using the correlation between H/V and array data, which allows us to understand the delta system better.

2 Geological Settings

The Llobregat is a 156.5 km-long Mediterranean river with a 4,950 km^2 catchment basin. Its headwaters are in the Eastern Pyrenees, and it outlets to the south of Barcelona city forming a delta plain after having crossed the Catalan Coastal Ranges. The waters (surface water and groundwater) from the Llobregat alluvial and deltaic plain represent a resource of capital importance for the sustainable development of the Barcelona metropolitan area (Vázquez-Suñé et al. 2006).

The Llobregat emerging delta plain (Fig. 1) is covered by the superficial sediments of Quaternary age related to the evolution of this part of the SW of the Mediterranean margin

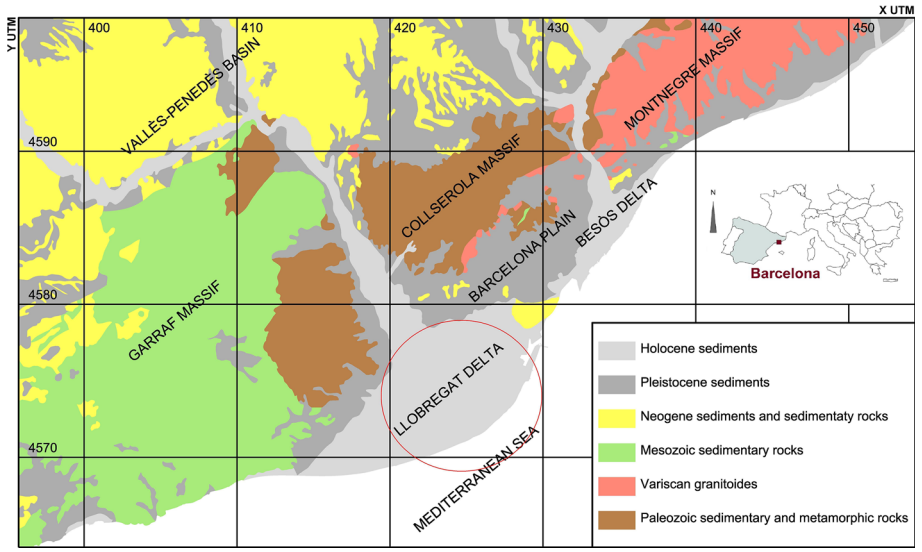

Fig. 1 Location of the study area (*red circle*) in a geological map of Barcelona region with some reference names (Llobregat and Besòs Deltas, Barcelona Plain, Collserola Massif). Map is shown in UTM coordinates, datum ETRS 89 31N

(Liquete et al. 2008; Gámez et al. 2009). According to these authors, the Quaternary sediments of the Llobregat delta are organised by the depositional sequences associated with the sea level changes during the Quaternary. These sequences are recorded in many coastal plains worldwide (Blum et al. 2013). The shallowest sediments of the emerging delta are linked to the global stabilization of the sea level that started approximately 9 kyr ago (Stanley and Warne 1994; Lambeck and Chappell 2001; Siddall et al. 2003). The thickness of such Quaternary sediments increases seawards, from approximately 20 m at the margin of the delta to approximately 100 m on the coastline (ICC-IGC-CUADLL 2006).

The Quaternary sediments of the emerging Llobregat delta plain overlie the Pliocene deposits, which are composed basically of grey marine marls with sandy layers. Borehole data (ICC-IGC-CUADLL 2006) indicate that the Pliocene deposits in the Llobregat delta reach a thickness of more than 200 m.

Offshore seismic profiles (Roca et al. 1999; García et al. 2011) indicate that near the coastline of the Llobregat delta, the Pliocene and the Quaternary deposits define a wedge-shaped succession prograding basinward up to 500 m thick. This succession includes several sequences related to the post Messinian (Plio-Quaternary) eustatic fluctuations that formed the modern Mediterranean continental shelves (Berné et al. 2004). The boundary between the Quaternary sequences and the Pliocene sequences in the Llobregat shelf is not well established. The Plio-Quaternary succession of the Llobregat delta rests unconformably on a faulted basement involving Palaeozoic, Mesozoic and Cenozoic rocks (Roca et al. 1999; Gaspar-Escribano et al. 2004; ICC-IGC-CUADLL 2006).

3 Previous Work on Passive seismic noise in the Llobregat Delta

Different microzonation studies were conducted in the city of Barcelona (Cid et al. 2001; Alfaro et al. 2001; Cadet et al. 2011). Some of these studies were based on the H/V seismic noise technique. In these previous studies, fundamental frequencies higher than 1 Hz were assigned to the Llobregat delta. As these results will be discussed in this work, the acquisition and processing parameters used by the authors are included as follows. In Alfaro et al. (2001), the seismic noise measurements were accomplished using a high dynamic range accelerometer (Altus K2 of Kinemetrics) with a flat response up to 50 Hz and a seismometer prototype with a flat response between 2 and 10 Hz. The seismic noise measurements were recorded for 180 s. The dataset was analysed in 20 s time windows. The H/V spectral ratio was computed in a range between 0.05 and 15 Hz. Cadet et al. (2011) used a Lennartz LE-3D 0.2 Hz triaxial sensor and a CityShark acquisition system to acquire seismic noise for 20 min using a sampling frequency of 100 Hz. In this case, the H/V spectral ratio was calculated in a frequency range between 0.5 and 20 Hz.

Furthermore, in the same study, seismic noise array measurements were made at 17 sites in Barcelona. Bedrock was not detected in the two seismic noise arrays corresponding to the Llobregat delta (Rugbi and Prat arrays shown in Fig. 2). According to the expected bedrock depth from geological information (Gámez et al. 2009), the soil fundamental frequency in the Llobregat delta should be in a lower frequency range than the ones obtained in these previous studies.

To understand this discrepancy between the soil fundamental frequencies from previous work and geology, additional H/V measurements were distributed along the area; some of them were made very close to or directly at the drilling sites where the soil column geology is known (Fig. 2). The H/V measurements had been complemented with one seismic noise

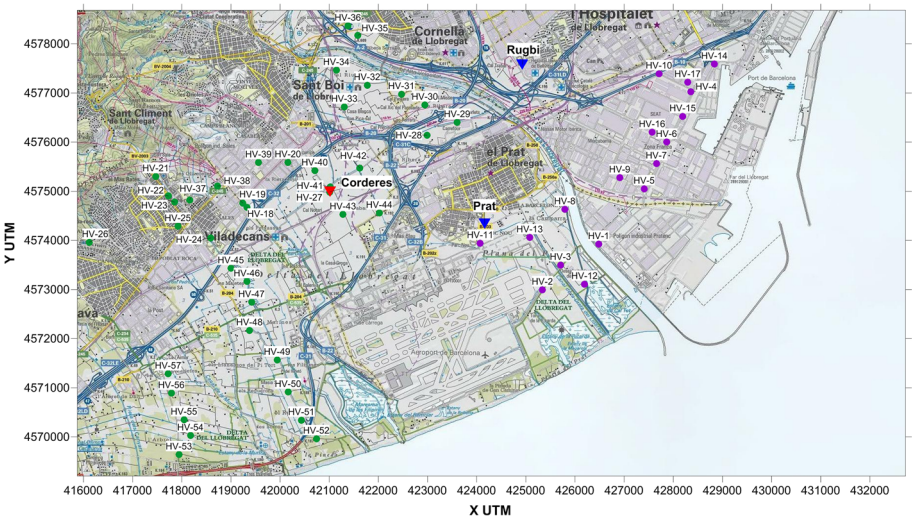

Fig. 2 Location of the geophysical measurements. The H/V stations are indicated by *green* and *purple circles*, these latter stations show the measurements carried out near boreholes with available stratigraphy (*HV-1* to *HV-17* corresponding to boreholes *BH-1* to *BH-17*). *Red triangle* indicates the location of the seismic noise array. Seismic noise array measurements conducted by Cadet et al. (2011) are shown in *blue triangles*. Map is presented in UTM coordinates, datum ETRS89 31N

array and active surface wave measurements to obtain a shear-wave velocity profile up to the bedrock (Fig. 2).

4 Seismic Noise Data Acquisition and Processing

4.1 The H/V Method

Fifty-seven new H/V measurements were distributed along the Llobregat delta (Fig. 2). Seventeen seismic noise stations were set up very close to or directly at the drilling sites with known shallow soil geology, to a maximum of approximately 70 m in depth.

The seismic ambient noise vibrations were recorded using a six-channel Cityshark datalogger connected to one Lennartz LE-3D 0.2 Hz triaxial sensor. The record length ranged between 10 and 20 min with a sampling frequency of 100 Hz. The H/V ratio was calculated using the Geopsy software (http://www.geopsy.org) developed during the SESAME project (http://sesame-fp5.obs.ujf-grenoble.fr), as follows in (1):

$$\frac{H}{V} = \frac{S_{\mathrm{NS}} + S_{\mathrm{EW}}}{2 * S_V} \tag{1}$$

where S_{NS}, S_{EW} and S_V are the magnitude of the smoothed Fourier spectrum of the north–south, east–west and vertical components, respectively. The Fourier spectrum of each component was smoothed in overlapped windows by 50 %. For further processing, only the quiet sections of the seismic noise recordings were used. Therefore, portions of the time sections with non-stationary signals have been removed by the STA/LTA anti-trigger algorithm (Lee and Stewart 1981). The length of the time series window was 60 s. The criteria for the interpretation of the H/V peaks have followed the SESAME guidelines (Bard and SESAME-Team 2004), such as:

1. The H/V peak amplitude (A_{HV}) should be higher than 2.
2. One frequency ($f\_$), lying between $f_{\mathrm{HV}}/4$ and f_{HV} (the soil fundamental frequency), exists, such that $A_{\mathrm{HV}}/A(f\_) > 2$, with $A(f\_)$ the H/V ratio amplitude at the frequency $f\_$.

4.2 The Array and Active Surface Wave Techniques

Seismic noise array and active surface wave measurements were made in the vicinity of a borehole that reaches the Pliocene materials up to 100 m in depth. The array equipment consisted of seven Lennartz LE-3D 0.2 Hz triaxial sensors and seven SARA SL06 seismic recorders. The sampling rate was fixed at 200 samples per second. This wireless equipment with GPS time allows recording the ground motion simultaneously. The sensors were arranged into two equilateral triangles with two different radii to a common centre where the seventh sensor was located. One triangle was rotated 60° with respect to the other one to obtain a good azimuthal coverage (Fig. 3). The investigation depth of a seismic noise array method depends on its radius (Okada 2003). To have a sufficient investigation depth, the observation arrays consist of multiple triangular arrays paired with different radii. After the first recording, the inner triangle was moved to a corresponding outer triangle with the same centre, and a second time window was acquired. This procedure was repeated by increasing the distance from the triangle vertex to the centre. Table 1 shows the radii of the

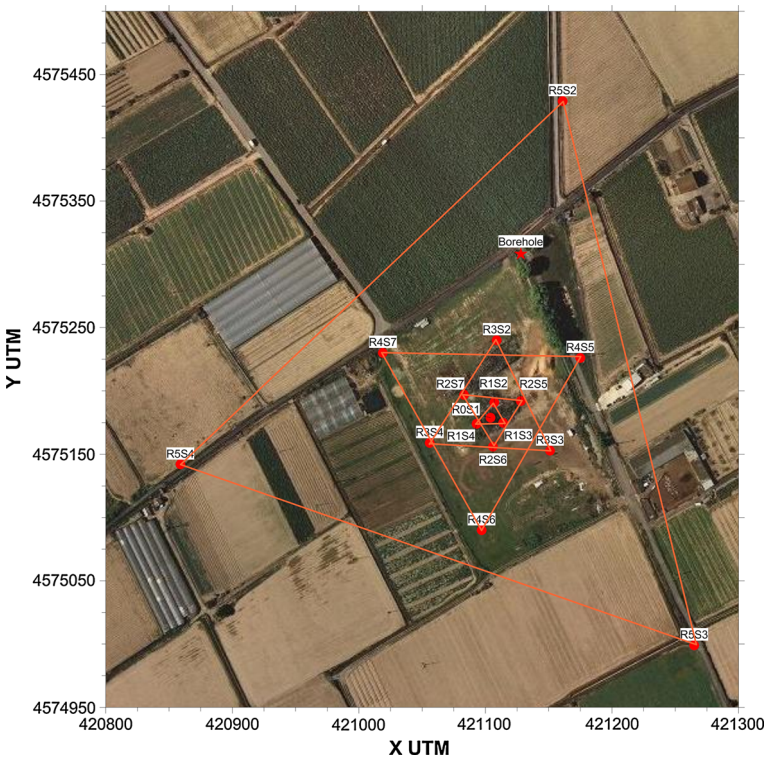

Fig. 3 Geometry used for the ambient noise array measurements performed in the Llobregat river delta; *red circles* indicate positions of stations. *Red star* indicates the location of the borehole. Map is shown in UTM coordinates, datum ETRS89 31N

Table 1 Radius and record length of the four arrays implemented in this study

Array	Name	Radius (m)	Record length (min)
Array 1	R1	10	25
	R2	25	
Array 2	R2	25	40
	R3	55	
Array 3	R3	55	110
	R4	100	
Array 4	R4	100	130
	R5	250	

triangles used in this study. The record length depends on the radii of the arrays: the larger the array aperture, the longer the record length (Table 1).

Complementary active surface wave measurements (MASW method) have been made to obtain a higher resolution in the near surface layers. We set up 24 sensors of 4.5 Hz distributed every 5 m in a linear geometry. A seismic profile was performed using a DMT seismic recorder. The active source was a 5 kg hammer striking a metal base plate. Two

shots were located on each side of the profile (at 5 and 7.5 m off-set). The record length was fixed at 1.5 s with a sampling interval of 0.25 ms.

The record of each seismic noise array measurement was analysed with the frequency–wave number (FK) and spatial autocorrelation (SPAC) methods to obtain the dispersion or autocorrelation curves. The FK method assumes that the surface waves contained in seismic noise propagate in a plane across the receiver setup (Lacoss et al. 1969; Horike 1985). The analysis of the dispersion characteristics of these waves is conducted in the frequency domain. First, the arrival time differences between the sensors are obtained using a test velocity vector (the velocity and the direction of propagation) and the relative position of the sensors. Second, the signals are shifted according to this delay and stacked in frequency domain. This process is repeated for the frequency, direction of propagation and velocity ranges. The resulting plot is called a beam power (Capon 1969). To retrieve the dispersion curve of the surface waves, a search for the maximum beam power is performed. Another approach to analyse seismic noise is the spatial auto-correlation technique SPAC (Aki 1957; Ohori et al. 2002; Roberts and Asten 2004). The SPAC technique assumes that the distribution of sources in the noise wavefield is random in time and space. That allows for applying a stochastic approach that does not attempt to identify individual sources. The seismic noise processing includes calculating the spatial autocorrelation curves between the sensor pairs. The average of the autocorrelation ratios is linked to the dispersion curve. Like in the H/V method, the processing of seismic noise array data has been conducted by following the guidelines proposed by the SESAME research group and using the Geopsy package (http://www.geopsy.org). The MASW data were also analysed with Geopsy using the FK method to retrieve the dispersion curve (DC).

5 Results

5.1 The H/V Method

The H/V ratio responses were obtained at each measurement point of the set of sites along the studied area. Two main different topologies of the H/V curves were obtained. Some sites show a clear single peak in the shape of H/V spectral ratio (Fig. 4a), whereas for the remaining locations, two clear peaks in the H/V spectral ratio curves are observed, one at low frequencies (<1 Hz) and the other at high ones (>1 Hz) (Fig. 4b, c). According to Lachet and Bard (1994), a sharp seismo-acoustic impedance contrast (>2) between layers is required to produce a peak in the H/V ratio. The frequency value of the first maximum of the H/V spectral ratio represents the soil fundamental frequency of a site, and it is related to the impedance contrast between the soft sedimentary cover and the bedrock. Usually, only one peak is observed in the H/V spectral ratio, but in some cases, two clear peaks in the H/V curves can be obtained, such as the results shown previously. Therefore, a large acoustic contrast (density and shear-wave velocity) between two superficial layers could cause the second soil resonance measured in the study area.

However, in the literature, peaks at higher frequencies are rarely studied in detail (Guéguen et al. 1998; Le Brun et al. 2001; Picozzi et al. 2009). The higher resonance frequencies are related to a shallower impedance contrast caused by a superficial layer, which can behave independently of the entire soil column. Nevertheless, geological and geophysical (e.g., boreholes with lithological descriptions or shear-wave velocity profiles) data are especially needed to better explain the presence of this second peak, which normally is neglected. Usually, this information is not available.

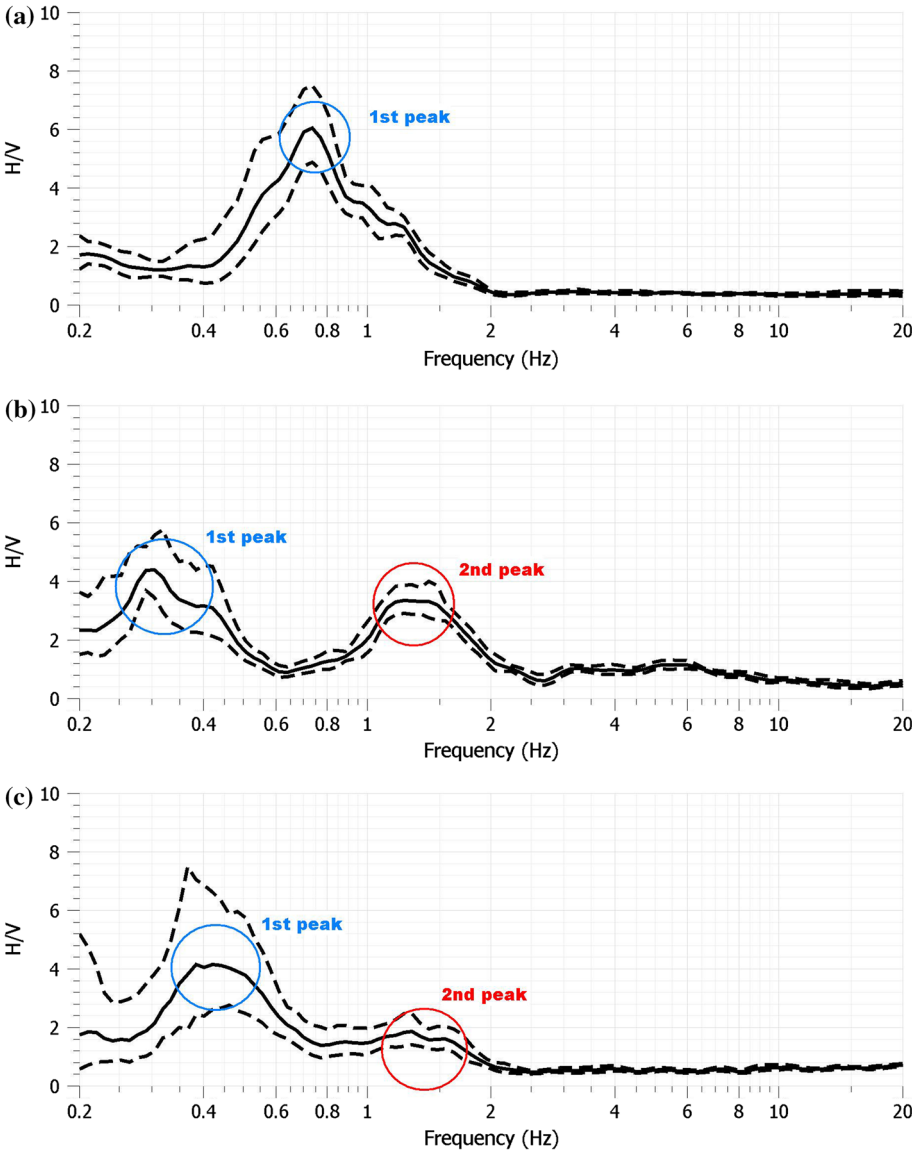

Fig. 4 Topology of the H/V curves observed in the study area: **a** single peak site, showing a clear peak (HV-17); **b** double peak site; characterised by the presence of two peaks, (HV-11); **c** same as **b** but with the second peak not fully significant (amplitude lower than 2), (HV-12). Soil fundamental frequency would correspond to the 1st H/V peak. The H/V average spectral ratio is represented by a *black solid line*, *dashed lines* indicate the associated standard deviations

Figure 5 shows the soil fundamental frequency and the frequency of the second peak in the H/V spectrum throughout the study area. The soil fundamental frequency ranges between 0.3 and 14.6 Hz, and the frequency range of the second peak is from approximately 1.1–2.6 Hz. The values and distribution of the second peak frequency fit well with

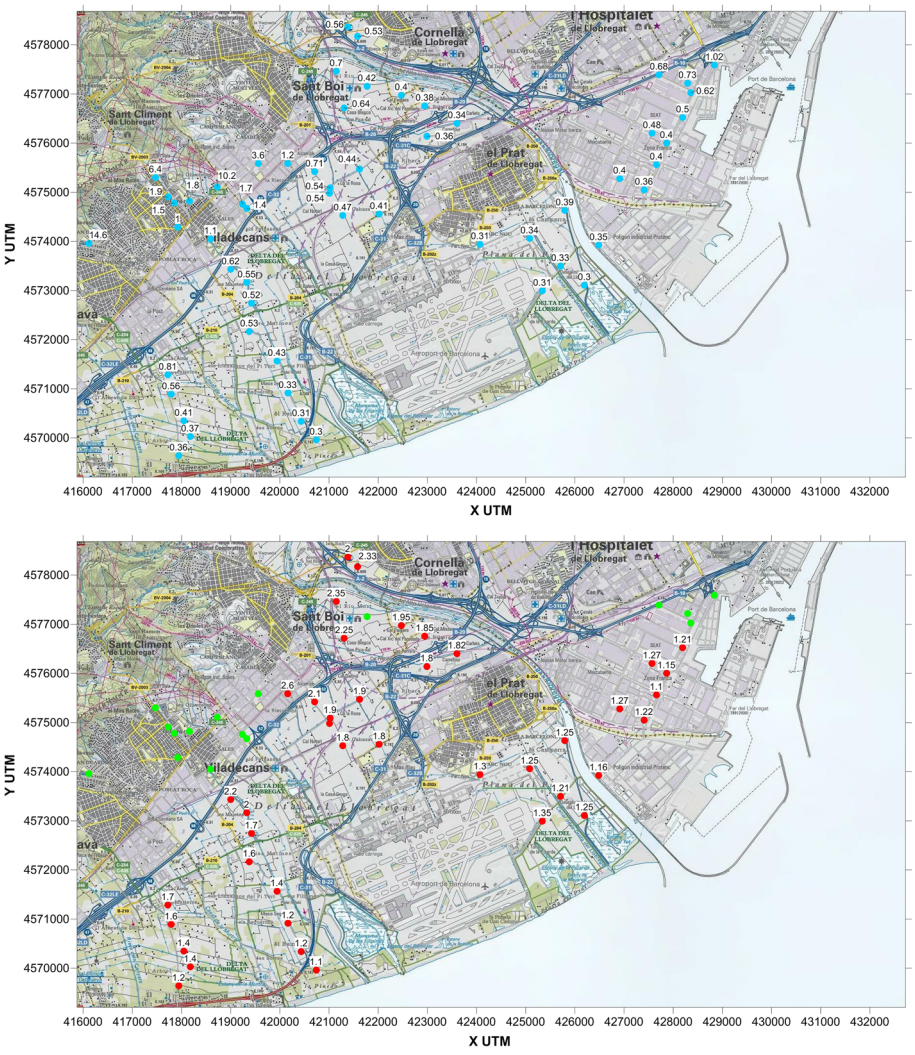

Fig. 5 Results derived from the H/V spectrum throughout the study area. *Top* soil fundamental frequency values. *Bottom* second peak frequency values. Points without labels (*green circles*) indicate sites without a second peak. Map is shown in UTM coordinates, datum ETRS89 31N

the Quaternary geology, as we will show next. The H/V ratio site responses obtained were compared with the shallow geology from the boreholes (Fig. 6). It has been found that the sites with two clear peaks in the H/V spectral ratio (HV-1, HV-2, HV-3, HV-6, HV-8, HV-9, HV-11, HV-12 and HV-13) have a significant clay layer overlying a gravel deposit. The clay thickness ranges between 10 and 40 m and extends over the Llobregat delta, but it thins northeastward until it disappears (ICC-IGC-CUADLL 2006; IGC 2013); in this sector, only one peak can be obtained (HV-4, HV-10, HV-14, and HV-17).

The H/V curves showing a second peak with an amplitude lower than 2 (Fig. 4c) could correspond to a transition zone from a sector characterised by a distinctive clay–gravel

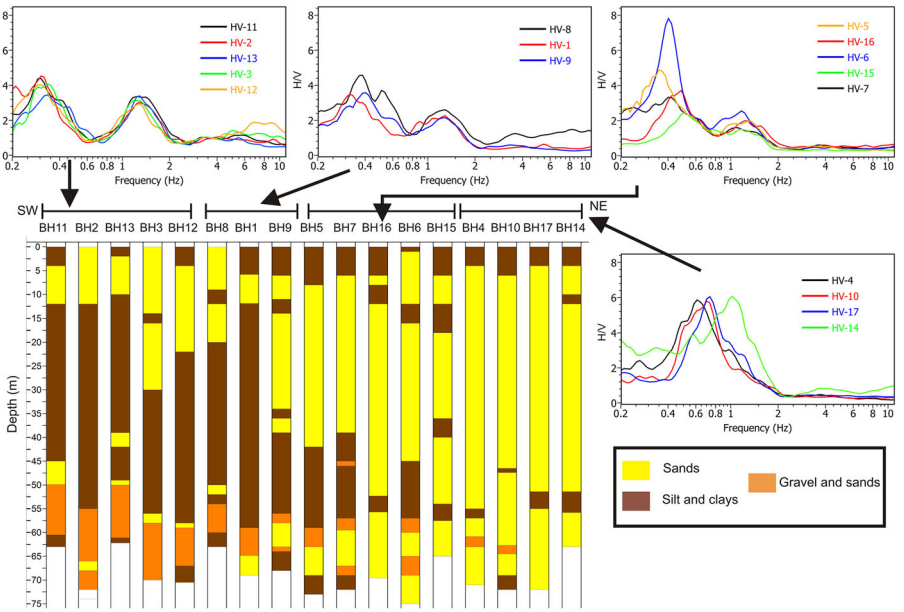

Fig. 6 Boreholes profiles sorted from *SW* to *NE*; geological layers are identified in legend. The H/V spectra corresponding to the measurements carried out at each borehole. The spectra have been grouped according to their topology

contact to another one where this contact is lacking (HV-5, HV-7, HV-15, and HV-16). On the basis of this ground truth, we can state that the presence of the second peak in the H/V spectral ratio may be caused by the presence of the clay–gravel contact. To confirm that, we obtain a shear-wave velocity profile to identify not only the soil/bedrock contact but also the main acoustic impedance contrasts within the quaternary column.

5.2 The Array and Active Surface Wave Techniques

As the first step of array data processing, the H/V seismic noise analysis was performed at each measurement station to evaluate the hypothesis of a horizontally stratified soil structure. The same shape of the H/V curves over the entire frequency band implies a 1D stratified soil structure. An example of the H/V curves corresponding to different stations with a 25–55 m array aperture is shown in Fig. 7. In this case, the H/V curves show the same shape over the entire frequency band, the soil fundamental frequency is 0.54 Hz, and a second peak of approximately 2.0 Hz is observed. For all of the seismic noise array measurement locations, the soil fundamental frequency ranges between 0.52 and 0.58 Hz, and the frequency of the second peak varies between 1.8 and 2.0 Hz (Table 2). This minimum variation of the frequency peaks indicates that the hypothesis of a horizontally stratified soil structure is accepted.

The outputs of FK computations for each array configuration are shown in Fig. 8. The minimum and maximum wave number limits for each array are determined from their theoretical array response (Wathelet 2005). The dispersion curve is used only between $k_{min}/2$ (k_{min} is the resolution limit of the array) and k_{max} (k_{max} being the aliasing limit of the array) (the exponential curves in Fig. 8). Figure 8e shows the FK spectrum obtained from

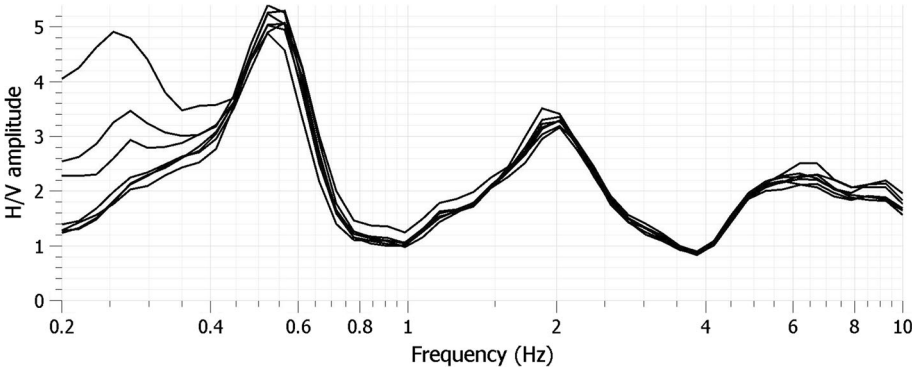

Fig. 7 The H/V curves corresponding to different stations for the 25–55 m array aperture. For all locations, the soil fundamental frequency value is 0.54 Hz and a second peak around 2.0 Hz is observed

Table 2 Soil fundamental frequency ($f0$) and second peak frequency ($f2$) values for all the seismic noise array measurement locations

Station name	f_0 (Hz)	f_2 peak (Hz)
R0S1	0.54	2.0
R1S2	0.54	1.9
R1S3	0.55	2.0
R1S4	0.55	2.0
R2S5	0.54	2.0
R2S6	0.54	2.0
R2S7	0.54	2.0
R3S2	0.53	1.9
R3S3	0.53	1.9
R3S4	0.54	2.0
R4S5	0.52	1.9
R4S6	0.54	1.9
R4S7	0.55	2.0
R5S2	0.55	2.0
R5S3	0.52	1.8
R5S4	0.58	1.9

the active surface wave data (MASW). The dispersion curve from active experiments covers a range of higher frequency than the dispersion curves from seismic noise data. An example of the results of SPAC calculations is shown in Fig. 9a. In this case, the high coherence between both results is supported by a good agreement between the FK dispersion curve and the maxima in the SPAC histogram (Fig. 9b).

The dispersion curves obtained with each array configuration are joined together with the dispersion curve from the active MASW method to obtain a unique dispersion curve to be inverted (Fig. 10). The standard deviation for each frequency was obtained from the FK histogram for the passive data, and considering the dispersion of high amplitude energy in the FK plot for the active part. As a result, the dispersion curve spans over a broad frequency range from 1 to 30 Hz. The Rayleigh wave velocities range from 1,000 m/s at the low frequency to 200 m/s at high frequencies. The resulting dispersion curve exhibits a pronounced hump of approximately 2 Hz that needs to be carefully analysed before

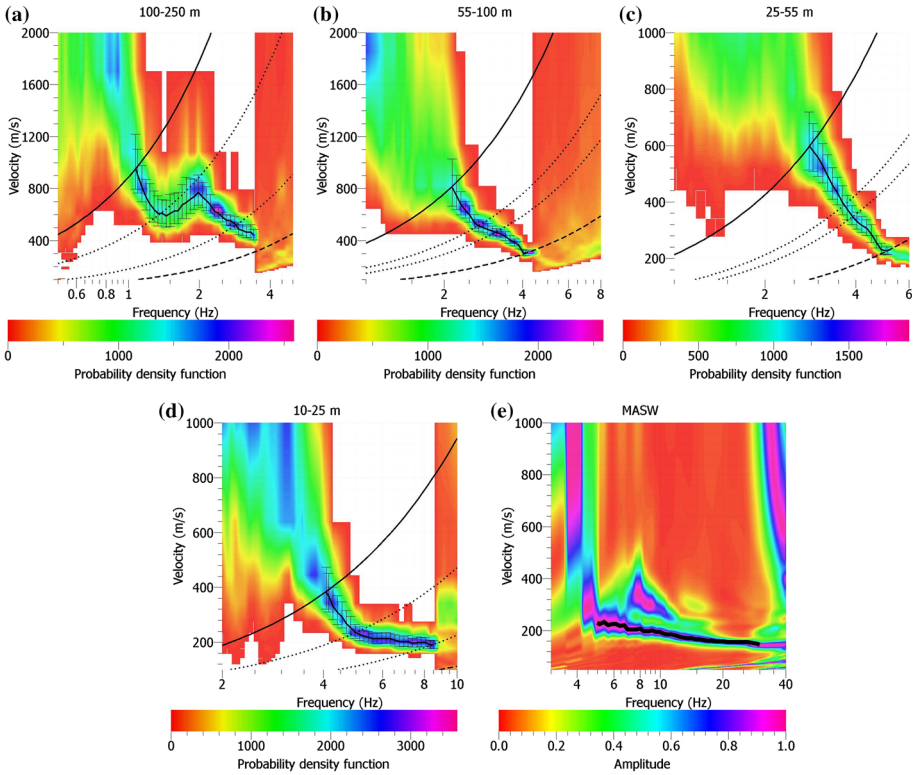

Fig. 8 FK histograms (*colour scale*) with the selected dispersion curve (*black*) for all the array apertures **a**–**d**. Exponential curves show the theoretical response of the array defining the resolution (*continuous line*) and aliasing (*dashed line*) limits. **e** FK spectrum of the shot gather corresponding to the active surface wave measurements (MASW method) applied in the Llobregat river delta

inversion. One possibility is that this anomaly in the dispersion curve is related to the expected velocity inversion within the soil column (De Nil 2005; Foti et al. 2003). According to Ikeda et al. (2010), in a velocity inversion profile, the first higher mode of dispersion curve is predominant in a frequency range. Under these conditions, the observed dispersion curve is a combination of the fundamental and the first higher modes. On the basis of these results, we can establish that the DC hump most likely belongs to the first higher mode. This behaviour should be taken into account during the inversion process. To eliminate the effect of the first higher mode, the dispersion curve between 1.5 and 2.4 Hz was not included in the inversion process.

In contrast, the SPAC autocorrelation curves from each array have been jointly inverted. The inversion processing of the dispersion curve from FK and the SPAC autocorrelation curves has been done with Dinver software included in the Geopsy package based on a neighbourhood algorithm process (Wathelet et al. 2004; Wathelet 2005). The inversion of the dispersion and autocorrelation curves is performed assuming that the layering in the subsurface is horizontal, as has been tested with the H/V method.

The results obtained from the H/V method have been used as constraints to obtain the 1D inversion model of shear-wave velocity. As a basic model parameterization, two soft layers over a half-space model are selected, which is consistent with the analysis of the

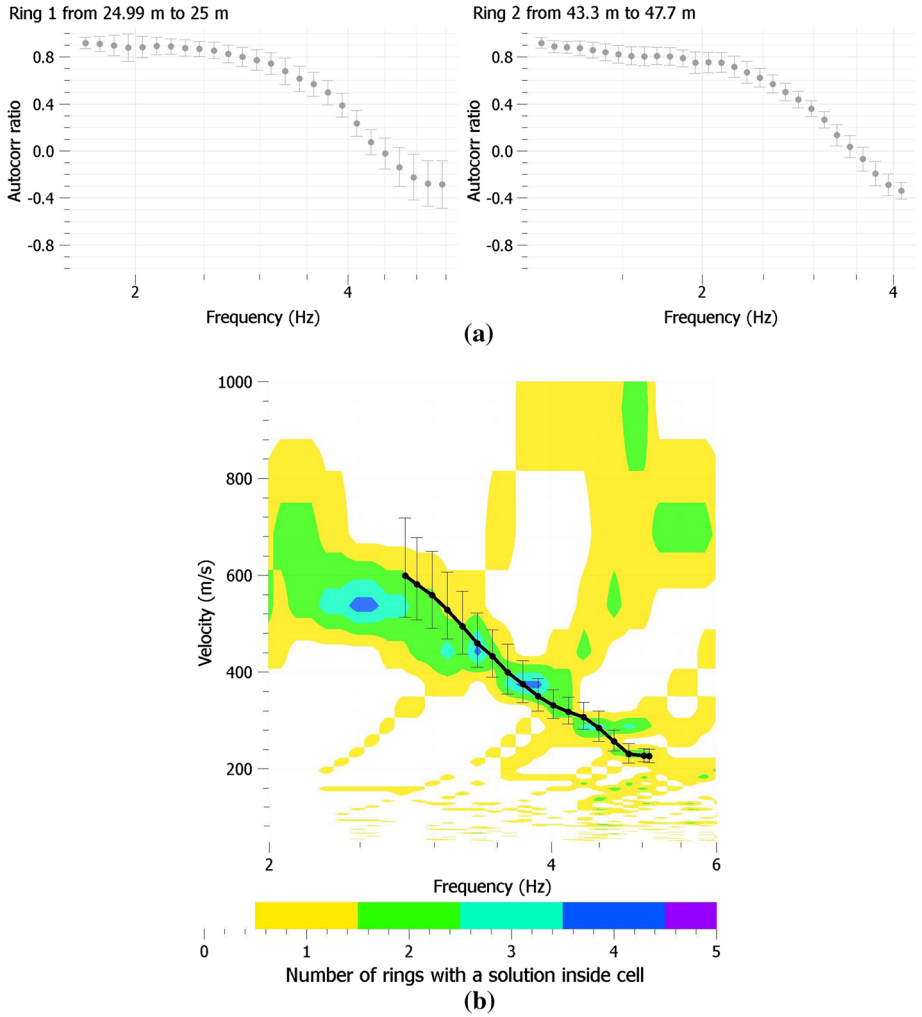

Fig. 9 **a** Autocorrelation curves from SPAC method. Examples with 25–55 m array aperture are shown. **b** Comparison between histogram from SPAC method (*colour scale*) and dispersion curve from FK analysis (*black curve with error bars*) for the same array aperture

H/V peak frequencies. A third layer is added to take into account the velocity inversion detected in the dispersion curve (Fig. 10). Therefore, the soil profiles are represented by three soil layers over the bedrock. The compressional and shear-wave velocities in each layer are uniform except in the first layer, where a power law velocity increase is assumed. This power law fits better with the gradual change observed in the dispersion curve for the higher frequency range (Fig. 10). The parameter range for P-wave and S-wave in the second and third layers allows for the velocity inversion.

Figures 11 and 12 show the match between the experimental curves (the black lines with error bars) from FK and SPAC methods, respectively, and the modelled dispersion and autocorrelation curves (colour coded) corresponding to the shear-wave velocity models resulting from the inversion. For the whole dispersion curve, the overall shape of the curve

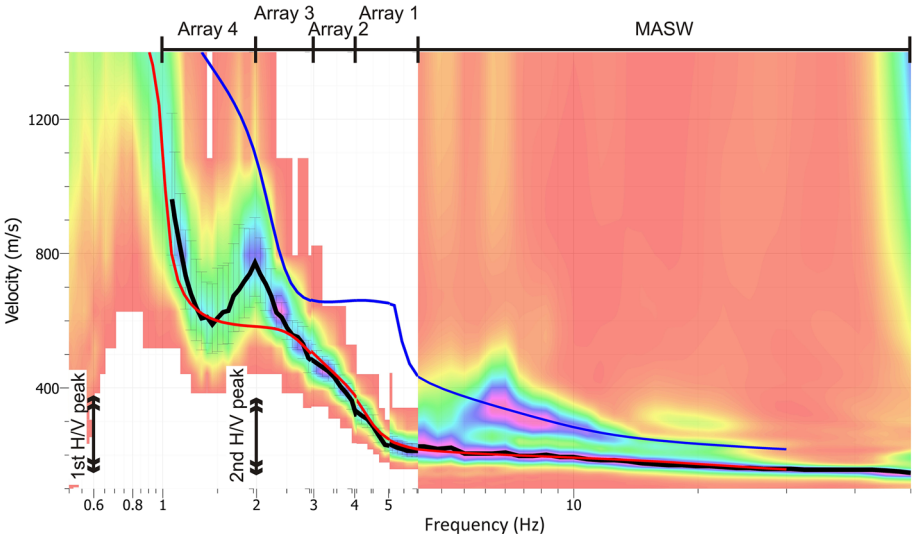

Fig. 10 Combined dispersion curve from each dispersion curve shown on Fig. 8 (*black line*). Theoretical dispersion curves of fundamental (*red*) and first higher modes (*blue*) computed using shear-wave profile obtained from the inversion of the dispersion curve

fits well. Moreover, for most rings, the experimental and modelled autocorrelation curves match.

Shear-wave velocity models (V_s) from the surface to the bedrock have been obtained from the seismic noise array analysis (Fig. 13). For both FK and SPAC methods, the soil profiles are similar. The models with a minimum misfit obtained from the FK and SPAC analyses are coherent in general (Table 3), with the main difference in the base depth of the third layer.

To constrain the interpretation, the inversion models were compared with a lithological description corresponding to the Corderès borehole located 120 m northeast of the array centre (Fig. 14). The first soil layer approximately 25 m thick and a mean shear-wave velocity of 220 m/s can be related to a mixture of clay, silt and sand according to the borehole description. Underneath this layer, a gravel and sand stratum that reaches approximately 80 m in depth (according to drilling) is observed. That would correlate with a layer of mean shear-wave velocity ranging between 890 and 1,250 m/s. Note that this gravel stratum is characterised by a high shear-wave velocity. The V_s properties can be explained by the dependency of V_s on the degree of compaction of the material due to the weight of the overlaying material. Havenith et al. (2007) showed that the V_s of the gravels changes with the thickness of the sediment cover, as a thicker gravel deposit shows a higher V_s. In our case, a high V_s value can be expected as its thickness is significant. Beneath this second layer, a soft layer can be formed with marls on top that can be related to a mean shear-wave velocity of approximately 630 m/s. The impedance contrast between the second and third layers produces a strong velocity inversion, which can be seen in the dispersion curve (Fig. 10). Considering the information from the borehole, the bottom of the third layer reaches at least 100 m in depth. Taking the information provided by the array into account, this layer reaches up to 300 m in depth at least. This result cannot be confirmed by any geological data. Considering the high shear-wave velocity (approximately 2,200 m/s) in the last layer, it can be interpreted as the bedrock or the seismic basement. In summary, both V_s models are coherent with the soil column description of the

Fig. 12 Comparison between measured autocorrelation curves obtained with SPAC processing method (*black lines and error bars*) and modelled autocorrelation curves (*coloured lines*) corresponding to the V_s models resulting from autocorrelation curves inversion. *Error* misfit is colour code

borehole (the first 100 m). The main difference between the FK and SPAC results is the bedrock depth. To discern which is the optimal model, the theoretical dispersion and the H/V curves will be obtained in the next section.

At the present time, there is no global agreement about the penetration depth of a seismic noise array. For example, the maximum investigation depth reached at each array can be calculated from the maximum wavelength (λ_{max}) divided by 3 (Cadet et al., 2011). λ_{max} is obtained by multiplying the low-frequency limit of the dispersion curve by the corresponding phase velocity. In our case, the low-frequency limit of the dispersion curve is 1.1 Hz, and the corresponding phase velocity is 1,000 m/s. Then, λ_{max} is 1,100 m and the maximum investigation depth would be 365 m. In contrast, Park et al. (1999) considered a penetration depth of the order of half λ_{max} for surface waves; therefore, the penetration depth of the array would be 550 m. In either case, these values are higher than the depth where the bedrock is detected.

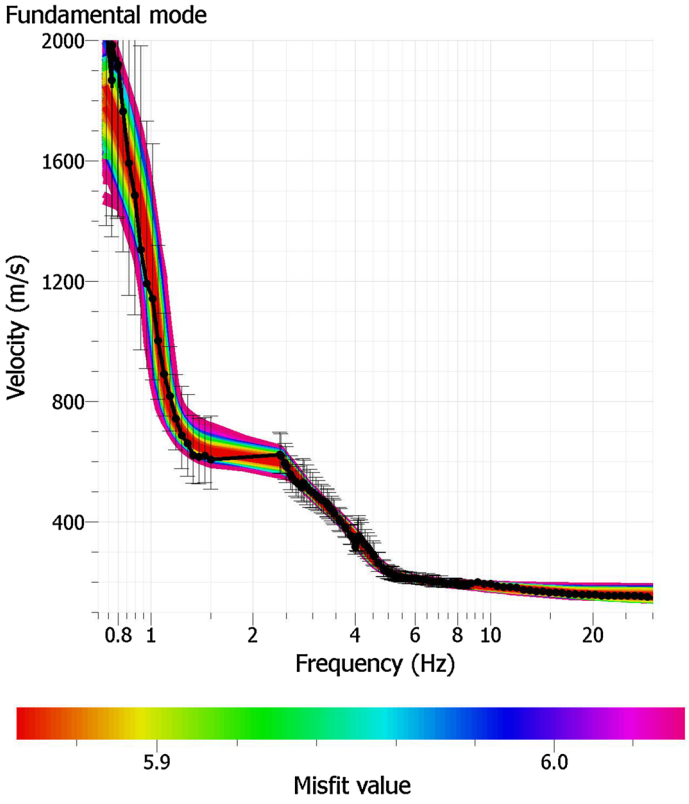

Fig. 11 Comparison between measured dispersion curve obtained with FK processing method (*black lines and error bars*) and modelled dispersion curves (*coloured lines*) corresponding to the V_s models resulting from DC inversion. *Error* misfit is colour code

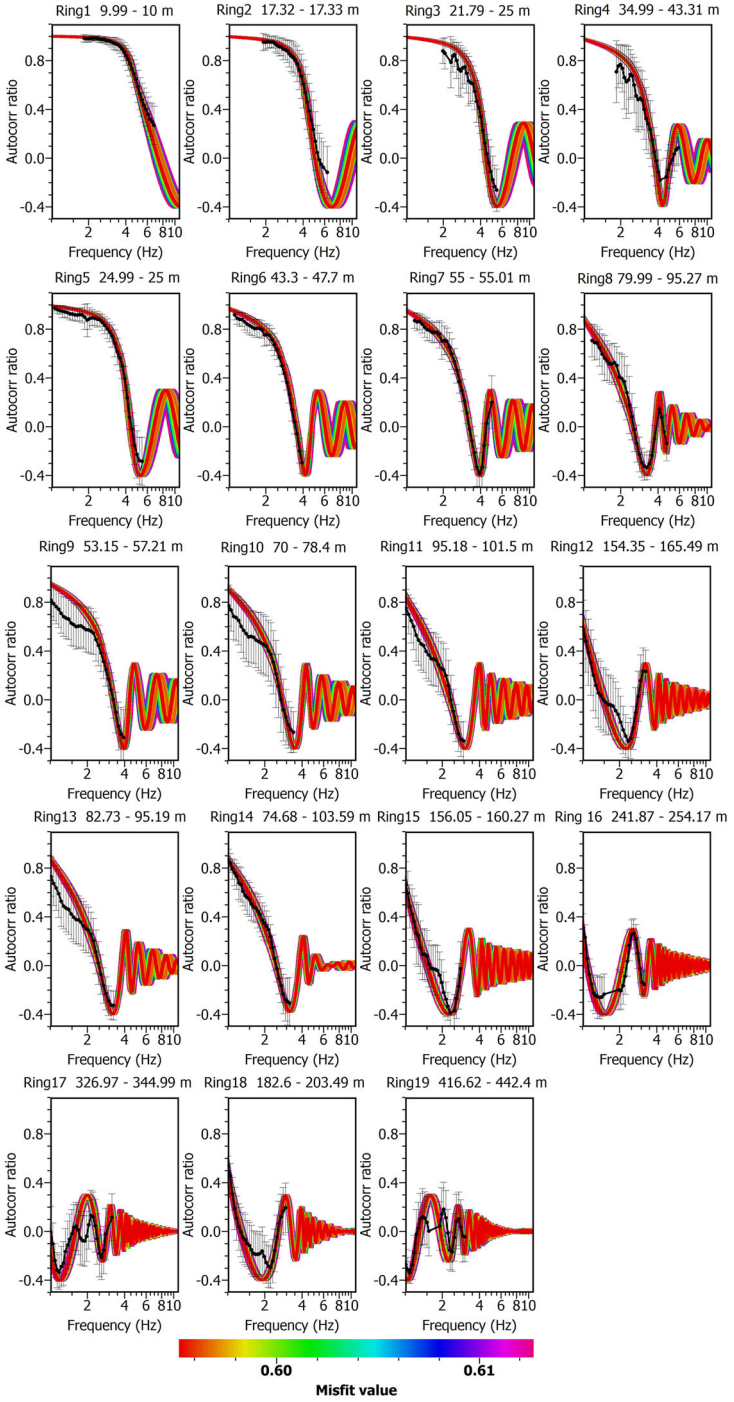
Ring1 9.99 - 10 m
Ring2 17.32 - 17.33 m
Ring3 21.79 - 25 m
Ring4 34.99 - 43.31 m
Ring5 24.99 - 25 m
Ring6 43.3 - 47.7 m
Ring7 55 - 55.01 m
Ring8 79.99 - 95.27 m
Ring9 53.15 - 57.21 m
Ring10 70 - 78.4 m
Ring11 95.18 - 101.5 m
Ring12 154.35 - 165.49 m
Ring13 82.73 - 95.19 m
Ring14 74.68 - 103.59 m
Ring15 156.05 - 160.27 m
Ring 16 241.87 - 254.17 m
Ring17 326.97 - 344.99 m
Ring18 182.6 - 203.49 m
Ring19 416.62 - 442.4 m
Autocorr ratio
Frequency (Hz)
0.60
0.61
Misfit value

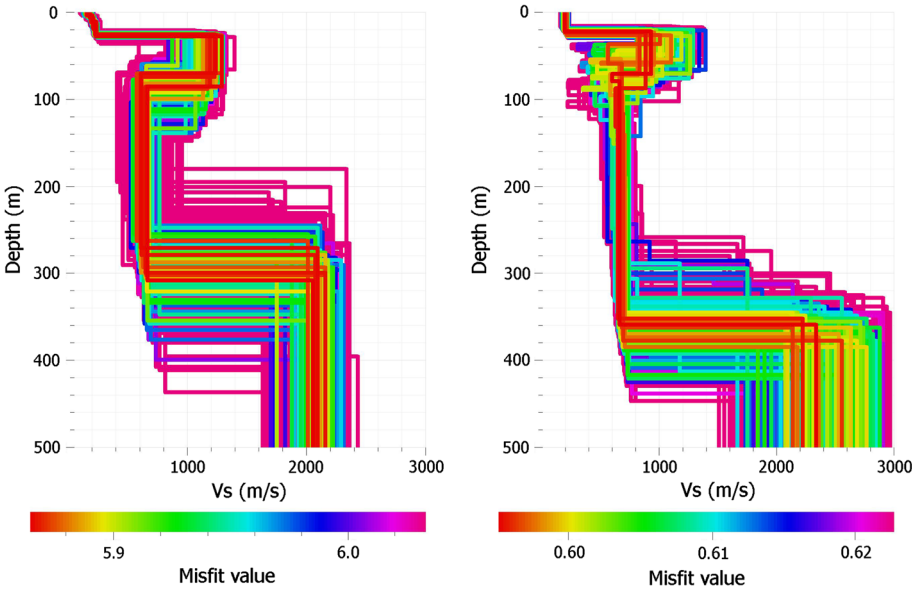

Fig. 13 *Left* Shear-wave velocity profiles obtained from the inversion of dispersion curve from both passive and active experiments. Misfit is lower than 5.87. *Right* Shear-wave velocity profiles obtained from the inversion of the autocorrelation curves with a misfit lower than 0.63

Table 3 Shear-wave velocity models (V_s) from surface to bedrock obtained by FK and SPAC analysis and inversion processing

	Description	FK		SPAC	
		Thickness (m)	V_s (m/s)	Thickness (m)	V_s (m/s)
First layer	Very soft	25	220	25	220
Second layer	Stiff	48	1,250	62	890
Third layer	Soft	227	630	263	630
Fourth layer	Very stiff	∞	2,200	∞	2,400

6 Modelling

To understand the shape of the H/V ratio and validate the results obtained from the array technique, the theoretical H/V ratios are retrieved using the V_s models from both FK and SPAC analyses as input. A DC-forward software included in the Geopsy package is used to compute the theoretical horizontal-to-vertical spectral ratios (TH/V) shown in Fig. 15. A DC-forward computation is based on the eigenvalue problem described by Thomson (1950) and Haskell (1953) and subsequently modified by Knopoff (1964), Dunkin (1965) and Herrmann (1994). As expected with the presence of two high impedance contrasts in the S-wave velocity profile, one deep ($\geq$300 m in depth) and the other shallow ($\sim$25 m in depth), two levels of amplification are observed in the theoretical H/V spectra, one at low frequencies (approximately 0.55 Hz) and the other at high frequencies (approximately 2.0 Hz). These results are consistent with the frequency values of the maximum amplitude

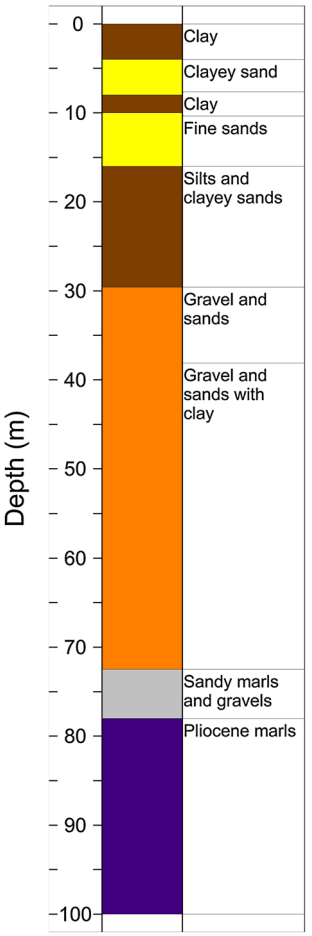

Fig. 14 Lithological description of soil column describing the borehole located 120 m northeast of the array centre

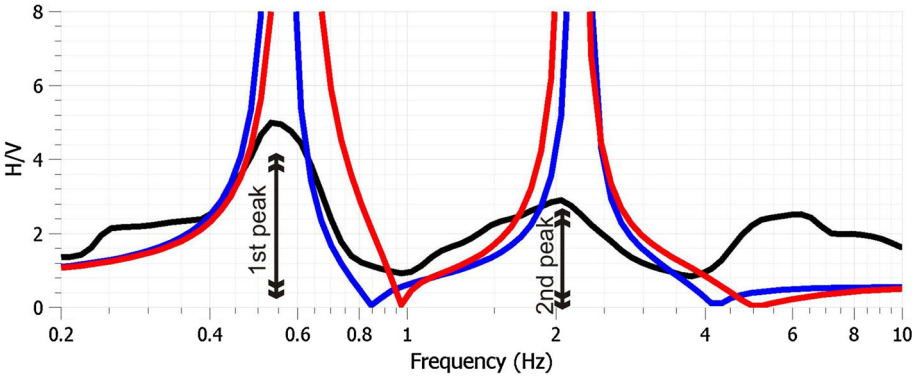

Fig. 15 The theoretical H/V ratio at the array centre considering the models obtained in the FK analysis (*red curve*), the SPAC analysis (*blue curve*) and the H/V curve obtained from seismic noise recorded in the centre of the array (*black curve*)

in the experimental H/V spectral ratio, 0.54 and 2.0 Hz, respectively (Fig. 7). In particular, the soil fundamental frequency obtained by the SPAC analysis (0.54 Hz) fits better than the value obtained from the FK analysis (0.61 Hz). Regarding the second peak, the differences between the two models are minimal. Therefore, the V_s profiles from the array technique explain the peaks observed in the H/V spectral ratio. The peak at higher frequencies (approximately 2 Hz) is related to the clay–gravel contrast, and the peak at lower frequencies (approximately 0.55 Hz) is associated with the contact between the third layer (composed of marls on top) and the bedrock.

In addition, the theoretical dispersion curves corresponding to the fundamental and the first higher modes have been computed using the Geopsy package. These curves have been overlapped on the experimental FK plots from the array and MASW data to understand the origin of the observed energy maxima (Fig. 10). The theoretical fundamental mode fits well with the experimental dispersion curve in the entire frequency range except in the interval between 1.5 and 2.4 Hz, where the energy maximum of the FK histogram is shifted towards the first higher mode. In contrast, the theoretical first higher mode curve is coherent with the second clear maximum observed in the FK plot between 7 and 10 Hz and the phase velocity approximately 300 m/s. This analysis validates the V_s model obtained from the array and MASW survey.

7 Discussion and Conclusions

The results from this study show that the structure of shallow Quaternary layers can clearly change the shape of H/V ratio, producing secondary peaks in some situations. This could affect the soil fundamental frequency identification that can produce errors in a site-effects evaluation or in the calculation of the bedrock depth in a geophysical exploration survey. Therefore, it is critical to estimate a preliminary soil fundamental frequency from the prior knowledge of geology. In this way, a suitable record length or seismometer natural frequency can be fixed during fieldwork planning. In addition, the applications of other exploration or modelling methods together with the H/V technique can help to avoid misinterpretations of the soil fundamental frequency in this type of environments.

Furthermore, in this paper, we have shown that a detailed study of the full H/V shape can provide information about surface geology. Regarding site-effect studies, the presence of two clear peaks in the H/V spectral ratio means two important impedance contrasts between layers. Therefore, a significant amplification of seismic waves produced by these contrasts can be expected at these locations. Moreover, secondary peaks can have a noticeable impact where low rise constructions are predominant, as they are more sensitive to high frequencies. The distribution of secondary peaks has to be included in microzonation studies, as the zonation of soil fundamental frequency does not fit the highest damage observed in some cases, in contrast to the general expectation (Guéguen et al. 1998).

Taking into account these new results obtained in this work from seismic noise processing and modelling, the high values of soil frequencies (>1 Hz) obtained from the Barcelona seismic microzonation (Alfaro et al. 2001; Cadet et al. 2011) are related to the clay–gravel contact present in the Llobregat river delta, not to the bedrock.

Concerning geological studies in a deltaic environment, analysing the H/V topology is useful in delineating the clay–gravel contact and defining the transition zones between sectors with different quaternary geology. This knowledge is critical to the groundwater management in the Llobregat delta.

We have demonstrated the utility of the array technique as an exploration tool in areas with a velocity inversion in the soil structure. For example, the seismic refraction tomography method has significant intrinsic limitations due to the presence of a high-velocity layer over a low velocity, in this case, gravel over marl. In addition, the P-wave seismic records from deltaic areas are marked by large zones lacking seismic penetration, which has been attributed to the presence of shallow gas and which is long regarded as a nuisance because of the extreme low seismic resolution and penetration (Missiaen et al. 2002). Under these conditions, the array technique has become very useful due to the low attenuation of surface waves in presence of gas as well as the logistical advantages of using seismic noise.

The V_s models obtained from the array and MASW survey have been validated in the modelling section. First, the two theoretical H/V peaks fit well with the experimental H/V peaks. Second, the theoretical dispersion curves are coherent with the observed maxima in the FK plot.

Finally, we have shown that the array and the H/V techniques are suitable for urban environments where other geophysical techniques are limited by anthropic noise and logistic issues, providing the 3D mapping of the quaternary layers and bedrock geometry.

The subsoil characteristics of the Llobregat river delta are representative of the geology found in many areas on the Mediterranean coast, as its geological structure is subject to the Mediterranean Sea level changes. The study conducted in this paper will be useful in interpreting the H/V spectral ratio in these areas, as similar shapes are expected.

Acknowledgments The fieldwork has been made possible with the help of the students who collaborated with the Geophysical Techniques Group of ICGC (Institut Cartogràfic i Geològic de Catalunya). We thank L. V. Socco for her constructive comments about higher modes. We would like to thank especially the anonymous reviewers for their contributions to improving this paper.

References

Aki K (1957) Space and time spectra of stationary stochastic waves, with special reference to microtremors, Tokyo University. Bull Earthq Res Inst 25:415–457

Alfaro A, Goula X, Susagna T, Pujades LG, Navarro M, Sánchez J, Canas JA (2001) Preliminary map of soil predominant periods in Barcelona by using Microtremors. Pure appl Geophys 158:2499–2511

Asten MW, Henstridge JD (1984) Array estimators and use of microseisms for reconnaissance of sedimentary basin. Geophysics 49:1828–1837

Bard PY (1999) Microtremor measurements: a tool for site effect estimation? In: Irikura K, Kudo K, Okada H, Sasatani T (eds.) The effects of surface geology on seismic motion—recent progress and new horizon on ESG study, Balkema, Rotterdam 3:1251–1279

Bard PY (2008) The H/V technique: capabilities and limitations based on the results of the SESAME project. Bull Earthq Eng 6:1–2

Bard PY, SESAME-Team (2004) Guidelines for the implementation of the H/V spectral ratio technique on ambient vibrations-measurements, processing and interpretations, SESAME European research project EVG1-CT-2000-00026, deliverable D23.12, http://www.sesame-fp5.obs.ujf-grenoble.fr. Accessed June 2013

Benjumea B, Teixidó T, Martínez P, Valls P. (2006) High-resolution seismic methods on unconsolidated sediments: examples from fluvial-deltaic areas in Catalonia. Proceedings of V Asamblea Hispano Portuguesa de Geodesia y Geofísica. http://www.igc.cat/web/ca/igc_pubtec_2005_2006.html. Accessed July 2014

Benjumea B, Macau A, Gabàs A, Bellmunt F, Figueras S, Cirés J (2011) Integrated geophysical profiles and H/V microtremor measurements for subsoil characterization. Near Surf Geophys 9(5):413–425

Berné S, Rabineau M, Flores JA, Sierro FJ (2004) The impact of Quaternary global changes on strata formation: exploration of the shelf edge in the northwest Mediterranean Sea. Oceanography 17(4):92–103

Blum M, Martin J, Milliken K, Gavin M (2013) Paleovalley systems: insights from Quaternary analogs and experiments. Earth Sci Rev 116:128–169
Bonnefoy-Claudet S, Cornou C, Bard PY, Cotton F, Moczo P, Kristek J, Fäh D (2006) H/V ratio: a tool for site effects evaluation. Results from 1-D noise simulations. Geophys J Int 167:827–837
Bonnefoy-Claudet S, Baize S, Bonilla LF, Berge-Thierry C, Pasten C, Campos J, Volant P, Verdugo R (2009) Site effect evaluation in the basin of Santiago de Chile using ambient noise measurements. Geophys J Int 176:925–937
Cadet H, Macau A, Benjumea B, Bellmunt F, Figueras S (2011) From ambient noise recordings to site effect assessment: the case study of Barcelona microzonation. Soil Dynam Earthq Eng 31:271–281
Capon J (1969) High-resolution frequency-wavenumber spectrum analysis. Proc IEEE 57:1408–1418
Castellaro S, Mulargia F (2009) The effect of velocity inversion on H/V. Pure appl Geophys 166:567–592
Chatelain JL, Guillier B, Cara F, Duval AM, Atakan K, Bard PY, the WP02 SESAME team (2008) Evaluation of the influence of experimental conditions on H/V results from ambient noise recordings. Bull Earthq Eng 6:33–74
Cid J, Susagna T, Goula X, Chavarria L, Figueras S, Fleta F, Casas A, Roca T (2001) Seismic zonation of Barcelona based on numerical simulation of site effects. Pure appl Geophys 158:2559–2577
Custodio E (2012) Low llobregat aquifers: intensive development, salinization, contamination, and management. The llobregat. Springer, Berlin, pp 27–49
De Nil D (2005) Characteristics of surface waves in media with significant vertical variations in elastodynamic properties. J Environ Eng Geophys 10(3):263–274
Delgado J, López Casado C, Giner J, Estévez A, Cuenca A, Molina S (2000) Microtremors as a geophysical exploration tool: applications and limitations. Pure appl Geophys 157:1445–1462
Dunkin JW (1965) Computation of modal solutions in layered, elastic media at high frequencies. Bull Seismol Soc Am 55(2):335–358
Fäh D, Kinf F, Giardini D (2001) A theoretical investigation of average H/V ratios. Geophys J Int 145:535–549. doi:10.1046/j.1365-246X.2001.01406.x
Falgàs E, Ledo J, Benjumea B, Queralt P, Marcuello A, Teixidó T, Martí A (2011) Integrating Hydrogeological and Geophysical methods for the characterization of a deltaic aquifer system. Survey Geophys. doi:10.1007/s10712-011-9126-2
Foti S, Sambuelli L, Socco VL, Strobbia C (2003) Experiments of joint acquisition of seismic refraction and surface wave data. Near Surface Geophysics 1(3):119–129
Gabàs A, Macau A, Benjumea B, Bellmunt F, Figueras S, Vilà M (2014) Combination of geophysical methods to support urban geological mapping. Surv Geophys 35(4). doi:10.1007/s10712-013-9248-9
Gámez D, Simó JA, Lobo FJ, Barnolas A, Carrera J, Vázquez-Suñé E (2009) Onshore–offshore correlation of the Llobregat deltaic system, Spain: development of deltaic geometries under different relative sea-level and growth fault influences. Sediment Geol 217:65–84
García M, Maillard A, Aslanian D, Rabineau M, Alonso B, Gorini C, Estrada F (2011) The Catalan margin during the Messinian salinity crisis: physiography, morphology and sedimentary record. Mar Geol 284:158–174
Gaspar-Escribano JM, Garcia-Castellanos D, Roca E, Cloetingh S (2004) Cenozoic vertical motions of the catalan coastal ranges (NE Spain): The role of tectonics, isostasy, and surface transport)
Goded T, Buforn E, Macau A (2012) Site effects evaluation in Málaga city's historical centre (Southern Spain). Bull Eartq Eng 10:813–838
Guéguen P, Chatelain JL, Guillier B, Yepes H, Egred J (1998) Site effect and damage distribution in Pujili (Ecuador) after the 28 March 1996 earthquake. Soil Dynam Earthq Eng 17:329–334
Haghshenas E, Bard PY, Theodulidis N, the SESAME WP04 team (2008) Empirical evaluation of microtremor H/V spectral ratio. Bull Eartq Eng 6:75–108
Haskell NA (1953) The dispersion of surface waves on multilayered media. Bull Seismol Soc Am 43(1):17–34
Havenith HB, Fäh D, Polom U, Roullé A (2007) S-wave velocity measurements applied to the seismic microzonation of Basel, Upper Rhine Graben. Geophys J Int 170:346–358
Herrmann RB (1994) Computer programs in seismology, vol IV, St Louis University
Horike M (1985) Inversion of phase velocity of long-period microtremors to the S-wave-velocity structure down to the basement in urbanized areas. J. Phys. Earth 33:59–96
Ibs-Von Seht M, Wohlenberg J (1999) Microtremor measurements used to map thickness of soft sediments. Bull Seismol Soc Am 89(1):250–259
ICC-IGC-CUADLL (2006) Mapa hidrogeològic del tram baix del Llobregat I el seu delta 1:30.000. Ed: Institut Cartografic de Catalunya-Institut Geològic de Catalunya-Comunitat d'Usuaris d'Aigües del Delta del Riu Llobregat

IGC (2013) Mapa geològic de les zones urbanes 1:5.000. Map sheets 287-128 (Almeda) and 288-128 (Bellvitge). Institut Geològic de Catalunya. www.igc.cat
Ikeda T, Matsuoka T, Tsuji T, Hayashi K (2010) Higher modes of surface waves in microtremor analysis, SEG Annual meeting, Denver, Colorado, pp 2034–2038
Jie S, Guangwen J, Denghai B, Jinge L, Lifeng W (2000) The noise interference of magnetotelluric sounding data. Geophys Geochem Explor 24(2):119–127
Knopoff L (1964) A matrix method for elastic wave problems. Bull Seismol Soc Am 54(1):431–438
Kühn D, Dahm T, Ohrnberber M, Vollmer D (2010) Imaging a shallow salt diaper using ambient seismic vibration beneath the densely built-up city area of Hamburg, Northern Germany. J Seism 15(3):507–531
Lachet C, Bard PY (1994) Numerical and theoretical investigations on the possibilities and limitations of the Nakamura's technique. J. Phys. Earth 42:377–397
Lacoss RT, Kelly EJ, Toksöz MN (1969) Estimation of seismic noise structure using arrays. Geophysics 34:21–38
Lafuerza S, Canals M, Casamor JL, Devincenzi JM (2005) Characterization of deltaic sediment bodies based on in situ CPT/CPTU profiles: a case study on the Llobregat delta plain, Barcelona, Spain. Marine Geol 222:497–510
Lambeck K, Chappell J (2001) Sea-level change through the last glacial cycle. Science 292:679–686
Le Brun B, Hatzfeld D, Bard PY (2001) Site effect study in urban area: experimental results in Grenoble (France). Pure appl Geophys 158:2543–2557
Lee W, Stewart S (1981) Principles and applications of microearthquake networks. Advances in geophysics, supplement 2. Academic Press, New York
Lermo J, Chávez-García FJ (1993) Site effect evaluation using spectral ratios with only one station. Bull. Seism. Soc. Am. 83:1574–1594
Liquete C, Canals M, De Mol B, De Batist M, Trincardi F (2008) Quaternary stratal architecture of the Barcelona prodeltaic continental shelf (NW Mediterranean). Marine Geol 250(3–4):234–250
Missiaen T, Murphy S, Loncke L, Henriet JP (2002) Very high-resolution seismic mapping of shallow gas in the Belgian coastal zone. Cont Shelf Res 22:2291–2301
Nakamura Y (1989) A method for dynamic characteristics estimation of subsurface using microtremors on the ground surface. Q Rep Railw Tech Res Inst Tokyo 30:25–33
Nguyen F, Kemna A, Antonsson A, Engesgaard P, Kuras O, Ogilvy R, Gisbert J, Jorreto S, Pulido-Bosch A (2009) Characterization of seawater intrusion using 2D electrical imaging. Near Surf Geophys 7(5–6):377–390. doi:10.3997/1873-0604.2009025
Nogoshi M, Igarashi T (1970) On the propagation characteristics estimations of subsurface using microtremors on the ground surface. J Seism Soc Japan 23:264–280 (In Japanese with English abstract)
Nogoshi M, Igarashi T (1971) On the amplitude characteristics of microtremor, Part 2. J Seism Soc Japan 24:26–40 (In Japanese with English abstract)
Ohori M, Nobata A, Wakamatsu K (2002) A comparison of ESAC and FK methods of estimating phase velocity using arbitrarily shaped microtremor arrays. Bull Seism Soc Am 92:2323–2332
Okada H (2003) The microtremor survey method, geophysical monograph, vol 12. Society of Exploration Geophysicists, Tulsa
Park CB, Miller RD, Xia J (1999) Multichannel analysis of surface waves. Geophysics 64:800–808
Parolai S, Bormann P, Milkereit C (2002) New relationships between Vs, thickness of sediments and resonance frequency calculated by the H/V ratio of seismic noise for the Cologne area (Germany). Bull Seismol Soc Am 92:2521–2527
Picozzi M, Strollo A, Parolai S, Durukal E, Özel O, Karabulut S, Zschau J, Erdik M (2009) Site characterization by seismic noise in Istanbul, Turkey. Soil Dynam Earthq Eng 29(3):469–482
Roberts JC, Asten MW (2004) Resolving a velocity inversion at the geotechnical scale using the microtremor (passive seismic) survey method. Explor Geophys 35:14–18
Roca E, Sans M, Cabrera L, Marzo M (1999) Oligocene to Middle Miocene evolution of the central Catalan margin (northwestern Mediterranean). Tectonophysics 315:209–229
Siddall M, Rohling EJ, Almogi-Labin A, Hemleben Ch, Meischner D, Schmelzer I, Smeed DA (2003) Sea-level fluctuations during the last glacial cycle. Nature 423:853–858
Slater L, Binley AM, Daily W, Johnson R (2000) Cross-hole electrical imaging of a controlled saline tracer injection. J Appl Geophys 44(2–3):85–102. doi:10.1016/S0926-9851(00)00002-1
Stanley JD (2001) Dating modern deltas: progress, problems, and prognostics 1. Annual Rev Earth Planet Sci 29(1):257–294
Stanley DJ, Warne AG (1994) Worldwide initiation of Holocene marine deltas by deceleration of sea-level rise. Science 265(5169):228–231
Thomson WT (1950) Transmission of elastic waves through a stratified solid medium. J Appl Phys 21:89–93

Tokimatsu K (1997). Geotechnical site characterization using surface waves. In: Ishihara (ed), Proc. 1st intl. conf. earthquake geotechnical engineering, Balkema, 3:1333–1368

Vázquez-Suñé E, Abarca E, Carrera J, Capino B, Gámez D, Pool M, Simó T, Batlle F, Niñerola JM, Ibáñez X (2006) Groundwater modelling as a tool for the European water framework directive (WFD) application: the Llobregat case. Phys Chem Earth 31(17):1015–1029

Wathelet M (2005) Array recordings of ambient vibrations: surface-wave inversion. PhD thesis, Université de Liège, Belgium

Wathelet M, Jongmans D, Ohrnberger M (2004) Surface wave inversion using a direct search algorithm and its application to ambient vibration measurements. Near Surf Geophys 2:211–221